J. Fluid Mech. (1993), *vol.* 247, *pp.* 17–38

Copyright © 1993 Cambridge University Press

Flow in deformable porous media. Part 1 Simple analysis

By MARC SPIEGELMAN

Lamont-Doherty Geological Observatory of Columbia University, Palisades, NY 10964, USA

(Received 25 February 1991 and in revised form 14 July 1992)

Many processes in the Earth, such as magma migration, can be described by the flow of a low-viscosity fluid in a viscously deformable, permeable matrix. The purpose of this and a companion paper is to develop a better physical understanding of the equations governing these two-phase flows. This paper presents a series of analytic approximate solutions to the governing equations to show that the equations describe two different modes of matrix deformation. Shear deformation of the matrix is governed by Stokes equation and can lead to porosity-driven convection. Volume changes of the matrix are governed by a nonlinear dispersive wave equation for porosity. Porosity waves exist because the fluid flux is an increasing function of porosity and the matrix can expand or compact in response to variations in the fluid flux. The speed and behaviour of the waves depend on the functional relationship between permeability and porosity. If the partial derivative of the permeability with respect to porosity, $\partial k_\phi/\partial\phi$, is also an increasing function of porosity, then the waves travel faster than the fluid in the pores and can steepen into porosity shocks. The propagation of porosity waves, however, is resisted by the viscous resistance of the matrix to volume changes. Linear analysis shows that viscous stresses cause plane waves to disperse and provide additional pressure gradients that deflect the flow of fluid around obstacles. When viscous resistance is neglected in the nonlinear equations, porosity shock waves form from obstructions in the fluid flux. Using the method of characteristics, we quantify the specific criteria for shocks to develop in one and two dimensions. A companion paper uses numerical schemes to show that in the full equations, viscous resistance to volume changes causes simple shocks to disperse into trains of nonlinear solitary waves.

1. Introduction

Many geophysical processes can be described by the flow of a low-viscosity fluid through a viscously deformable, permeable matrix. Examples include the flow of partially molten rock through the Earth's convecting mantle and the flow of water or oil in compacting sediments. These processes have always been of great interest to earth scientists; however, it is only with the derivation of a system of conservation equations (McKenzie 1984; Scott & Stevenson 1984, 1986) that we have begun to understand the fluid dynamics underlying these processes.

These new equations are similar to those used for traditional porous flow with the important distinction that the matrix is viscously deformable. Allowing the matrix to deform introduces interesting new behaviour. As this paper and a companion one (Spiegelman 1993) will stress, much of this behaviour is readily understood by noting that the matrix can deform in two different ways. First, because the matrix can expand and compact to change the volume fraction of fluid, variations in fluid flux

can propagate through the matrix as porosity waves. Previous work has shown that these equations admit solutions for finite-amplitude solitary waves of permanent form and constant velocity (Scott & Stevenson 1984; Richter & McKenzie 1984). Most of the work on the solitary waves is concerned with the existence and properties of these waves and principally considers problems where the background porosity is constant, and there is no matrix shear or mass transfer between solid and liquid. Under these conditions, solitary wave solutions exist in one, two and three dimensions (Barcilon & Richter 1986; Scott & Stevenson 1986; Barcilon & Lovera 1989). The one-dimensional waves are not solitons (Barcilon & Richter 1986) and have been shown to be unstable in two dimensions and develop into the two-dimensional solitary waves. The ability of the two-dimensional solitary waves to drive matrix convection has also been addressed (Scott 1988; Daily & Richter 1989). The second mode of matrix deformation is incompressible shear. When the matrix shear is forced, it can produce large pressure gradients that control the flow of the fluid in the pores (Spiegelman & McKenzie 1987; Phipps Morgan 1987; Ribe 1988*b*). Alternatively, lateral variations in fluid content can cause the matrix to convect (Rabinowicz, Nicola & Vigneresse 1984; Scott & Stevenson 1989; Buck & Su 1989; Sotin & Parmentier 1989). Given the flow of fluid and matrix, additional work has considered the transport of heat and chemical tracers in deformable porous media (Brown 1988; Ribe 1985*b*, 1988*a*; Richter 1986; Richter & Daly 1989).

The existing literature illustrates the wide range of behaviour inherent in the governing equations. The previous work on the solitary waves, however, is principally mathematical and concerned with a few special cases, while the work that includes incompressible matrix shear is mostly concerned with geophysical modelling of magma migration, particularly at mid-ocean ridges. The significance of the nonlinear waves in geophysical problems is not well understood and a more general physical understanding of these equations is still needed to put these previous results into context. The purpose of this study is to develop a better understanding through a series of analytic and numerical solutions to simple model problems. This work is divided into two parts. Part 1 (this paper) rewrites the governing equations into more tractable forms that emphasize the two distinct modes of matrix deformation. This paper also develops a series of useful approximations that allow analytic solution of the governing equations. These approximate solutions demonstrate the basic time-dependent behaviour of the equations for a range of geometries and initial conditions, and illustrate the contributions of the specific terms in the equations. Using the insight afforded by the approximate analytic solutions. Part 2 (Spiegelman 1993) investigates and quantifies the behaviour of the full equations using numerical techniques.

2. General equations: conservation of mass and momentum

The equations governing the percolative flow of a low-viscosity fluid or 'melt' through a viscously deformable permeable matrix were derived independently by several workers (McKenzie 1984; Scott & Stevenson 1984, 1986; Fowler 1985). These equations were originally derived for the problem of magma migration in a convecting mantle, and much of the nomenclature stems from this application. These equations however are based on the more general work of Drew (1971, 1983) for interpenetrating two-phase flows. Here we use the formulation from McKenzie (1984). His work provides a detailed derivation and explains that these equations are a macroscopic description of two interpenetrating viscous fluids with vastly different

Variable	Meaning	Value used	Dimension
a	pore spacing (grain size)	10^{-3}	m
b	constant in permeability	100–3000	none
ζ	matrix bulk viscosity	$10^{18}-10^{21}$	Pa s
η	matrix shear viscosity	$10^{18}-10^{21}$	Pa s
μ	melt shear viscosity	1–10	Pa s
ρ_f	density of melt	2800	kg m^{-3}
ρ_s	density of matrix	3300	kg m^{-3}

TABLE 1. Values of parameters

viscosities. The melt is assumed to form an interconnected porous network distributed over some characteristic pore (or vein) spacing a. As a continuum approximation, these equations are valid for lengthscales much larger than a and smaller than any characteristic variation in porosity. Moreover, these equations assume that inertial effects are negligible for both the percolating melt phase and for creeping matrix deformation. Estimates for magmatic systems give Reynolds numbers $Re < 10^{-8}$ for the melt, and even smaller values for the matrix as long as the porosity is much smaller than the critical value at which the matrix disaggregates. Once inertial effects become important, however, a more general set of equations for fluidized beds is necessary (e.g. Didwania & Homsy 1981, 1982).

With these considerations, the equations governing conservation of mass and momentum can be written

$$\frac{\partial(\rho_f \phi)}{\partial t} + \nabla \cdot (\rho_f \phi \boldsymbol{v}) = \Gamma, \tag{1}$$

$$\frac{\partial[\rho_s(1-\phi)]}{\partial t} + \nabla \cdot [\rho_s(1-\phi)\, \boldsymbol{V}] = -\Gamma, \tag{2}$$

$$\phi(\boldsymbol{v}-\boldsymbol{V}) = \frac{-k_\phi}{\mu} \nabla \mathscr{P}, \tag{3}$$

$$\frac{\partial \mathscr{P}}{\partial x_i} = \frac{\partial}{\partial x_j}\eta\left(\frac{\partial V_i}{\partial x_j} + \frac{\partial V_j}{\partial x_i}\right) + \frac{\partial}{\partial x_i}(\zeta - \tfrac{2}{3}\eta)\, \nabla \cdot \boldsymbol{V} - (1-\phi)\, \Delta\rho g \delta_{i3}, \tag{4}$$

$$k_\phi \sim a^2 \phi^n / b, \tag{5}$$

where ρ_f is the density of the melt, ϕ is the volume fraction occupied by the melt (porosity), $\boldsymbol{v}$ is the melt velocity, and Γ is the rate of mass transfer from matrix to melt (melting rate). ρ_s is the density of the solid matrix, $\boldsymbol{V}$ is the matrix velocity, k_ϕ is the permeability, μ is the melt viscosity and $\mathscr{P} = P - \rho_f g z$ is the fluid pressure in excess of hydrostatic pressure. $\mathscr{P}$ is often referred to as the piezometric pressure, or hydraulic head. η and ζ are the matrix shear and bulk viscosities respectively, and $\Delta\rho = \rho_s - \rho_f$, g is the acceleration due to gravity, x is the horizontal Cartesian coordinate and z the vertical. Estimates of some parameters for magmatic systems are given in table 1.

Equations (1) and (2) conserve mass for the melt and matrix respectively. Equation (3) is conservation of momentum for the melt and governs the separation of melt from matrix. This equation is a modified form of Darcy's law, and the term $\phi(\boldsymbol{v}-\boldsymbol{V})$ arises from the requirement that these equations be frame invariant to a Galilean transformation (Drew 1983; McKenzie 1984). Equation (4) governs momentum conservation for the matrix, which is treated as compressible, highly

viscous fluid. Unlike equations for more general two-phase flows, (3) and (4) contain only a single pressure, $\mathscr{P}$, which is related to the fluid pressure P. This is consistent with the assumption that the fluid is percolating slowly and dynamic pressure fluctuations in the fluid phase are negligible (Drew 1983; McKenzie 1984). Scott & Stevenson (1986) define a solid pressure as $-\frac{1}{3}$ the trace of the solid stress tensor. That is, $P_s = \frac{1}{3}\sigma^s_{kk} = P - \zeta \nabla \cdot V$. This definition is useful for showing that volume changes of the matrix are related to the pressure difference between the solid and liquid. Except for differences in definitions and notation, however, the equations derived by McKenzie and Scott & Stevenson are identical.

Equation (5) gives the permeability as a nonlinear, scalar† function of the pore spacing a, porosity ϕ, and a dimensionless coefficient, b. Equation (5) is a convenient parameterization for a range of porosity/permeability relationships valid for small porosities ($\lesssim$ 10–20%). More specific relations can be found in standard texts on porous flow (e.g. Dullien 1979; Scheidegger 1974; Bear 1988). The actual functional form of the permeability, k_ϕ, is not particularly crucial to the following discussion except for the important requirements that both k_ϕ, and $\partial k_\phi / \partial \phi$ be increasing functions of porosity. Simple capillaric models for permeability show that a power law with $n = 2$–3 is a good approximation for permeabilities of real two-phase systems and satisfies this nonlinearity criterion. More detailed analysis of texturally equilibrated melt/solid networks gives similar results (Cheadle 1989; Von Bargen & Waff 1986).

3. Simplified equations: constant-viscosity, constant-density, potential form

Little progress has been made in solving (1)–(5) in their most general form. However, these equations can be made more tractable if we consider problems where the matrix viscosities are constant and the melt and matrix are taken to be individually incompressible (i.e. ρ_f and ρ_s are constant but not necessarily equal). If we set the matrix shear and bulk viscosities (η, ζ) to be constant, then (4) can be written

$$\nabla \mathscr{P} = -\eta \nabla \times \nabla \times V + (\zeta + \tfrac{4}{3}\eta) \nabla (\nabla \cdot V) - (1-\phi) \Delta \rho g \boldsymbol{k}. \tag{6}$$

Equation (6) shows that the pressure gradients that drive the flow of melt arise from three sources: volume-preserving matrix shear, volume changes of the viscous matrix and the differential buoyancy between melt and matrix. For constant viscosities, the pressure gradients due to the two modes of matrix deformation can be separated.

By writing the matrix velocity field in potential form

$$V = \nabla \times \boldsymbol{\Psi}^s + \nabla \mathscr{U}^s, \tag{7}$$

where $\mathscr{U}^s$ is the matrix scalar potential, we can also decompose V into incompressible and compressible components. It should be stressed that the 'compressible' component of the velocity field refers to the ability of the solid framework to expand or compact in response to the injection or extraction of fluid. Because the porosity can change, the matrix velocity can have a non-zero divergence even though the individual crystals that form the framework are incompressible. It is useful to define the isotropic strain rate or 'compaction rate' of the matrix as

$$\mathscr{C} = \nabla \cdot V. \tag{8}$$

† In this work, the permeability is assumed to be isotropic. More generally, a permeability tensor can be used with little change in notation.

Given these definitions and approximations, (1)–(5) can be rewritten solely in terms of the porosity ϕ and matrix deformation. Expanding (2) gives

$$\partial\phi/\partial t + (\nabla \times \boldsymbol{\Psi}^{\mathrm{s}} + \nabla \mathscr{U}^{\mathrm{s}}) \cdot \nabla\phi = (1-\phi)\mathscr{C} + \Gamma/\rho_{\mathrm{s}}. \tag{9}$$

Adding (1) and (2) and substituting (3) and (6) yields

$$-\nabla \cdot \frac{k_\phi}{\mu}(\zeta + \tfrac{4}{3}\eta)\nabla\mathscr{C} + \mathscr{C} = \nabla \cdot \frac{k_\phi}{\mu}[\eta \nabla \times \nabla^2 \boldsymbol{\Psi}^{\mathrm{s}} - (1-\phi)\Delta\rho g \boldsymbol{k}] + \Gamma \frac{\Delta\rho}{\rho_{\mathrm{s}}\rho_{\mathrm{f}}}. \tag{10}$$

Equations (7) and (8) imply

$$\nabla^2 \mathscr{U}^{\mathrm{s}} = \mathscr{C}, \tag{11}$$

and taking the curl of (6) gives

$$\nabla^4 \boldsymbol{\Psi}^{\mathrm{s}} = -\frac{\Delta\rho g}{\eta} \nabla \times \phi \boldsymbol{k}. \tag{12}$$

Equations (9)–(12) form a coupled system of hyperbolic, elliptic and bi-harmonic equations that can be solved using standard techniques. More importantly this decomposition explicitly distinguishes between the equations governing incompressible and compressible matrix flow and allows these equations to be solved sequentially. §4.3 shows that in the limit of small porosity, the two modes of deformation are completely decoupled. Scott (1988) also proposes a decomposition into a 'circulation' and 'separation' flux; however, these fluxes are just linear combinations of $\boldsymbol{v}$ and $\boldsymbol{V}$ and the equations do not decompose readily.

Equation (12) governs incompressible matrix shear and is Stokes equation for the creeping rotational flow of the matrix. Equations (9)–(11) govern compressible matrix flow and will be shown to form a nonlinear wave equation for the evolution of porosity and compaction rate. Equation (9) conserves porosity and states that porosity changes are caused by matrix advection and by the balance between volume changes and melting. Equation (10) governs volume changes of the matrix. Given $\mathscr{C}$, the compressible component of matrix flow is determined by (11).

Equation (10) arises naturally from the decomposition used here, but has not been recognized before. This equation states that the volume changes of the matrix are driven by the divergence of the melt separation flux and the volume change due to melting, i.e.

$$\mathscr{C} = -\nabla \cdot \phi(\boldsymbol{v} - \boldsymbol{V}) + \Gamma\Delta\rho/(\rho_{\mathrm{s}}\rho_{\mathrm{f}}). \tag{13}$$

Equation (10), however, has been rearranged to stress that it is an elliptic equation for the compaction rate. The right-hand side of (10) contains volume changes due to the divergence of the 'forced melt flux' and volume changes on mass transfer. The forced melt flux is driven principally by buoyancy forces. The left-hand side of (10) shows that these forcing terms change the volume (second term) and develop a resistive melt flux driven by pressure gradients induced by expansion and compaction of the viscous matrix.

The elliptic term in (10) is perhaps the most important term in the governing equations. Dimensional analysis shows that viscous resistance to volume changes only becomes significant when the melt flux varies over the compaction length

$$\delta = [k_\phi(\zeta + \tfrac{4}{3}\eta)/\mu]^{\frac{1}{2}}. \tag{14}$$

In many geological problems, δ is small (order 100–1000 m) and several authors (Ribe 1985*a*; Ribe & Smooke 1987; Scott & Stevenson 1989) have proposed that the first term in (10) can be neglected for most geological problems. Other workers (Buck &

Su 1989; Sotin & Parmentier 1989) have simply neglected this term altogether. This zero-compaction-length approximation reduces a potentially singular second-order equation to a zeroth-order equation. As is typical of elliptic equations, however, this term controls boundary-layer flows and the existence and behaviour of solitary waves. Moreover, because this term causes dispersion into long trains of solitary waves, it can have effects that extend over many compaction lengths. This behaviour will be demonstrated in detail in Part 2.

3.1. *Non-dimensionalization*

The compaction length is the natural lengthscale for any problem involving compressible matrix deformation. The natural velocity scale is the percolation velocity

$$w_0 = k_0 \Delta\rho g/(\phi_0 \mu), \tag{15}$$

where

$$k_0 \equiv k_\phi(\phi_0) = a^2 \phi_0^n / b \tag{16}$$

is the permeability at the reference porosity $\phi = \phi_0$. The percolation velocity is the velocity of the melt relative to the matrix for a system with uniform porosity ϕ_0 and with no matrix deformation.

These definitions suggest the following non-dimensionalization, where primes denote dimensionless variables:

$$\left.\begin{gathered} \phi = \phi_0 \phi', \quad k_\phi = k_0 k'_\phi, \quad (x, z) = \delta(x', z'), \\ \nabla = \nabla'/\delta, \quad (\boldsymbol{v}, V) = w_0(\boldsymbol{v}', V'), \quad \mathscr{C} = \frac{\phi_0 w_0}{\delta}\mathscr{C}', \\ (\boldsymbol{\Psi}^s, \psi^s, \mathscr{U}^s) = w_0 \delta(\boldsymbol{\Psi}'^s, \psi'^s, \mathscr{U}'^s), \quad t = \frac{\delta}{w_0} t', \quad \Gamma = \frac{\rho_s \phi_0 w_0}{\delta}\Gamma'. \end{gathered}\right\} \tag{17}$$

The remainder of these papers will consider at most two-dimensional solutions to (9)–(12). Substituting (17) into the two-dimensional equations and dropping primes yields

$$\partial\phi/\partial t + (\nabla \times \psi^s \boldsymbol{j} + \nabla \mathscr{U}^s) \cdot \nabla\phi = (1 - \phi_0 \phi)\mathscr{C} + \Gamma, \tag{18}$$

$$-\nabla \cdot k_\phi \nabla \mathscr{C} + \mathscr{C} = \nabla \cdot k_\phi \left[\frac{\xi}{\phi_0}(\nabla \times \nabla^2 \psi^s \boldsymbol{j}) - (1 - \phi_0 \phi)\boldsymbol{k}\right] + \frac{\Delta\rho}{\rho_f}\Gamma, \tag{19}$$

$$\nabla^2 \mathscr{U}^s = \phi_0 \mathscr{C}, \tag{20}$$

$$\nabla^4 \psi^s = -(\phi_0^2/\xi)(\partial\phi/\partial x), \tag{21}$$

$$k_\phi = \phi^n, \tag{22}$$

where ψ^s is the two-dimensional stream function and $\xi = \eta/(\zeta + \frac{4}{3}\eta)$ is the ratio of the matrix shear viscosity to the effective bulk viscosity. Henceforth all variables will be assumed to be dimensionless unless otherwise noted.

3.2. *Boundary conditions*

Boundary conditions for the matrix are the standard conditions for a single-phase, low-Reynolds-number compressible fluid (e.g. no-slip or free-stress boundaries). Boundary conditions for the melt phase (ϕ and $\mathscr{C}$) can be considered in terms of the melt separation flux

$$\boldsymbol{q} = -k_\phi[(\xi/\phi_0)(\nabla \times \nabla^2 \psi^s \boldsymbol{j}) + \nabla\mathscr{C} - (1 - \phi_0 \phi)\boldsymbol{k}]. \tag{23}$$

In general, conservation of mass requires that the normal flux across a boundary be continuous or balanced by a local source or sink. More specific flux boundary

conditions include impermeable, rigid and 'free flux' boundaries. At an impermeable boundary the normal flux is zero for one of two reasons. Either $k_\phi = 0$ or $\nabla\mathscr{P}\cdot\mathrm{d}\boldsymbol{S} = 0$ where $\mathrm{d}\boldsymbol{S}$ is the normal to the boundary. The second condition places constraints on the normal derivative of the compaction rate and is required if the permeability is discontinuous across a boundary. As an example, this sort of boundary occurs during the initial compaction of a constant-porosity layer on to an impermeable base (see Part 2, §2). Whether an impermeable boundary remains stable in time however, depends on whether the components of the forced flux enter or exit the boundary. For example, an impermeable cap overlying a two-phase region will lead to disaggregation unless the impinging flux is balanced by freezing ($\Gamma < 0$) (Sparks & Parmentier 1991; Spiegelman 1990, 1991). At a rigid boundary, $\mathscr{C} = 0$ and $\mathrm{D}_V\phi/\mathrm{D}t = \Gamma$, thus, in the absence of melting and matrix flow a rigid boundary is also a constant-porosity boundary. The flux at a rigid boundary need not be constant, however, as $\nabla\mathscr{C}$ is variable. Finally a free-flux boundary has $\nabla\mathscr{C}\cdot\mathrm{d}\boldsymbol{S} = 0$ and yields no resistance to volume changes for the normal flux. Given these definitions, the boundary condition at the interface between a pure solid and a two-phase region should be no slip (continuous velocity) for the matrix and impermeable for the melt. In contrast, the interface between a two-phase region and a pure melt is free stress for the matrix and free flux for the melt. For conditions on the tangential melt flux at a two-phase/liquid boundary see Saffman (1971).

4. Basic physics: simple analysis

The following sections present analytic solutions for a series of model problems that have been chosen to illustrate the basic behaviour of the governing equations. We first demonstrate the effects of forced incompressible matrix shear on the flow of melt. The second problem considers the behaviour of infinitesimal perturbations to constant-porosity solutions. Finally we introduce several approximations that are useful for demonstrating the basic time-dependent behaviour of nonlinear compressible flow.

4.1. *Incompressible two-phase flow: constant porosity, no melting*

If the porosity is set constant and there is no mass transfer between solid and liquid, the governing equations reduce to a simple form that can be solved analytically. If we set $\phi = \text{const.}$ and $\Gamma = 0$ (18)–(22) become

$$\mathscr{C}_0 = 0, \quad \mathscr{U}_0^{\mathrm{s}} = \text{const.}, \quad \nabla^4\psi_0^{\mathrm{s}} = 0, \tag{24}$$

and the two-phase problem reduces to solving a single biharmonic equation for the incompressible matrix flow. Given any solution for ψ_0^{s}, the dimensional pressure and melt stream function ψ^{f} are given by

$$\mathscr{P} = \eta\int\frac{\partial}{\partial x}(\nabla^2\psi_0^{\mathrm{s}})\,\mathrm{d}z - (1-\phi_0)\,\Delta\rho g z + \text{const.}, \tag{25}$$

$$\psi^{\mathrm{f}} = \psi_0^{\mathrm{s}} - (k_0/\phi_0\mu)\,[\eta\nabla^2\psi_0^{\mathrm{s}} - (-\phi_0)\,\Delta\rho g x]. \tag{26}$$

Therefore the flow of melt is completely determined by the flow of the matrix and gravity. These results are physically reasonable. If the individual solid and liquid phases are each incompressible, then fixing the porosity and having no melting implies that the two-phase system must be incompressible. As porosity is constant, the matrix shear can only be driven by the boundary conditions (or other sources of

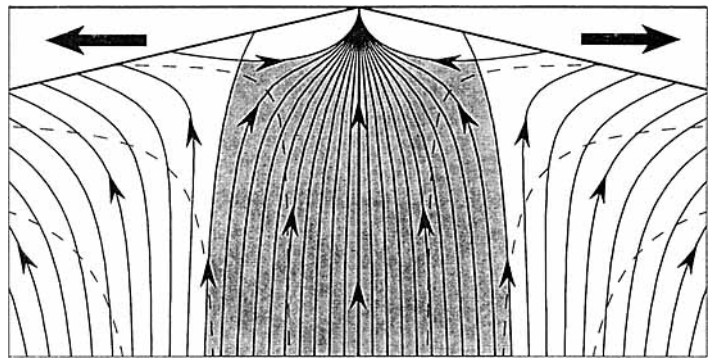

FIGURE 1. Melt and solid flow fields for an analytic solution for corner flow of an incompressible two-phase system. The two-phase region has constant porosity and no melting and is bounded on the top by two rigid boundaries spreading horizontally at a constant velocity. The matrix streamlines are dashed lines. The melt streamlines are solid with arrows showing the direction of melt transport. This solution shows that non-hydrostatic pressure gradients developed by the forced shear of the matrix can redirect the flow of melt. The strong focusing effect shown here is due to a singularity in the pressure associated with corner flow (Batchelor 1967). The shaded region is the set of all streamlines that connect the corner to depth. This solution is discussed in detail in Spiegelman & McKenzie (1987) and forms a simple model for melt extraction at mid-ocean ridges.

vorticity). The fluid in the pores, however, flows down pressure gradients due to buoyancy and viscous shear. If the vorticity $-\nabla^2\psi_0^s$ is significant, the flow of melt can be quite different from simple vertical percolation. As an example, figure 1 shows melt and matrix streamlines for a corner flow solution for the matrix that demonstrates significant focusing of melt streamlines due to incompressible matrix flow. Details of the corner flow solution can be found in Spiegelman & McKenzie (1987).

4.2. *Effects of non-constant porosity: linear analysis*

Relaxing the condition of constant porosity, this section uses linear analysis to illustrate the behaviour of infinitesimal perturbations to the constant-porosity solutions. This solution is useful for identifying the contribution and magnitude of each of the terms in the governing equations and, in particular, the elliptic term in (19). For clarity, we consider only perturbations to a uniform background flux in an infinite domain with no matrix shear deformation or melting. This geometry has been used extensively in studies of the nonlinear solitary waves and is a crude approximation to the corner flow solutions of figure 1 far from the corner.

Using the basic state that $\phi = 1$ (dimensionless), $\Gamma = 0$ and $V_0 = \nabla \times \psi_0^s \boldsymbol{j} = W_0 \boldsymbol{k}$ and introducing a small perturbation such that

$$\phi = 1 + \epsilon\phi_1, \quad \mathscr{C} = 0 + \epsilon\mathscr{C}_1, \quad \mathscr{U}^s = 0 + \epsilon\mathscr{U}_1^s, \quad \psi^s = W_0 x + \epsilon\psi_1^s, \tag{27}$$

the linearized two-dimensional equations to order ϵ are

$$\frac{\partial\phi_1}{\partial t} + W_0\frac{\partial\phi_1}{\partial z} = (1-\phi_0)\mathscr{C}_1, \tag{28}$$

$$-\nabla^2\mathscr{C}_1 + \mathscr{C}_1 = -[n(1-\phi_0) - \phi_0]\,\partial\phi_1/\partial z, \tag{29}$$

$$\nabla^2\mathscr{U}_1^s = \phi_0\mathscr{C}_1, \tag{30}$$

$$\nabla^4\psi_1^s = (\phi_0^2/\xi)\,(\partial\phi_1/\partial x), \tag{31}$$

$$k_1 = n\phi_1, \tag{32}$$

Note that the linearized equations (28) and (29) form a coupled set of equations for the porosity and compaction rate only. In this approximation, the matrix velocity is completely determined to first order once ϕ_1 and $\mathscr{C}_1$ are known.

As these equations are invariant to a Galilean transformation, W_0 can be set to zero without loss of generality. In this case, (28) and (29) can be combined to form a single wave equation for porosity:

$$\frac{\partial \phi_1}{\partial t} + v_0 \frac{\partial \phi_1}{\partial z} - \nabla^2 \frac{\partial \phi_1}{\partial t} = 0. \tag{33}$$

Here $v_0 = [n(1-\phi_0)-\phi_0](1-\phi_0)$ and the second term in (33) describes the propagation of porosity driven by the divergence of the forced background flux. The third term arises from the viscous resistance of the matrix to volume changes ($-\nabla^2 \mathscr{C}_1$ in (29)). If the viscous term is neglected (i.e. the matrix had no strength or $\delta \equiv 0$), then all perturbations would simply propagate vertically with permanent form at velocity v_0. As v_0 is greater than the melt velocity by approximately a factor of n, porosity waves can (and generally do) travel faster than the melt in the pores.

When the elliptic viscous resistance term is retained, travelling plane waves

$$\phi_1(\boldsymbol{k}, t) = A\, \mathrm{e}^{\mathrm{i}(\boldsymbol{k}\cdot x - \omega t)} \tag{34}$$

form solutions if ω satisfies the dispersion relationship

$$\omega = k_z v_0/(k^2+1) \tag{35}$$

where $k^2 = \boldsymbol{k}\cdot\boldsymbol{k}$.† This solution has also been found from another form of the equations (D. McKenzie, personal communication).

As ω is real and depends on $\boldsymbol{k}$, these solutions are dispersive. The phase velocity for a given wave vector $\boldsymbol{k}$ is ω/k or

$$c_{\mathrm{p}} = v_0 \cos\theta/(k^2+1), \tag{36}$$

where θ is the angle between the wave vector and the vertical. The group velocity, $\boldsymbol{c}_{\mathrm{g}} = \boldsymbol{\nabla}_k \omega$ is

$$\boldsymbol{c}_{\mathrm{g}} = -\frac{2v_0 k_x k_z}{(k^2+1)^2}\boldsymbol{i} + \frac{v_0}{k^2+1}\left[1 - \frac{2k_z^2}{k^2+1}\right]\boldsymbol{k} \tag{37}$$

and is plotted in figure 2.

Equation (36) shows that the maximum phase velocity is v_0. Thus viscous resistance to volume changes causes short-wavelength waves to propagate more slowly than those of longer wavelength. This is physically reasonable because it takes more effort to move a steep porosity gradient through a viscous medium than a more gradual gradient. Not surprisingly, the dispersion becomes most significant for wavelengths comparable to or less than the compaction length. The viscous compaction term also affects the speed and direction of wave packets. Figure 2 and (37) show that wave packets with $2k_z^2/(k^2+1) < 1$ (approximately, wavelengths longer than the compaction length) will travel faster than the background flux, while higher-frequency wave packets will move more slowly and can even move backwards relative to the matrix. Part 2 will show that this back-propagation of information can have significant effects for the nonlinear equations. Figure 2 also shows that wave packets inclined to the vertical ($k_x k_x \neq 0$) will have a horizontal component of motion. In particular, if the wave vector points to the right of vertical ($k_x k_z > 0$) the group velocity points to the left. These waves should move sideways as well as up.

† The wave vector is denoted by $\boldsymbol{k}$ to distinguish it from the unit vector in the z-direction $\boldsymbol{k}$.

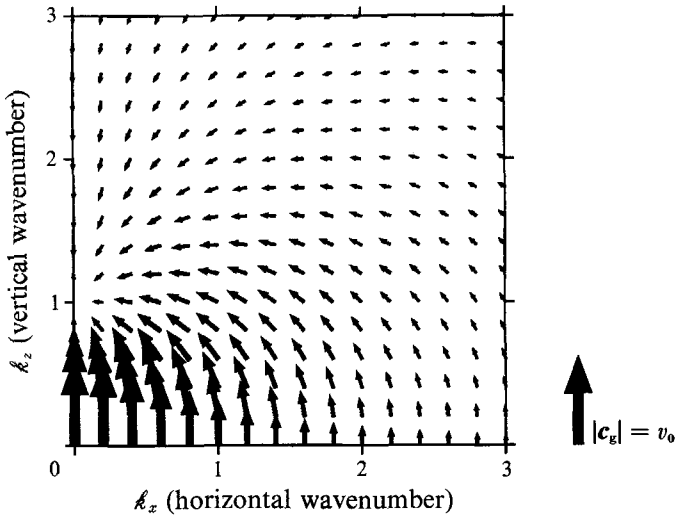

FIGURE 2. Group velocity, c_g as a function of wave vector k, for the dispersive plane-wave solutions of (33)

Both the dispersion of plane waves and the deflection of wave packets is caused solely by the elliptic compaction term. Another way to gain some insight into the effects of this term is to consider how it modifies the actual melt velocity. The perturbed melt velocity to first order is

$$v_1 = (\nabla \times \psi_1^s j + \nabla \mathscr{U}_1^s) + (\xi/\phi_0)(\nabla \times \nabla^2 \psi_1^s j) - \nabla \mathscr{C}_1 + [n(1-\phi_0) - (1+\phi_0)]\phi_1 k, \quad (38)$$

which is derived from (2)–(5) and the defined potentials. Given the plane wave solutions for ϕ_1, solutions for the other first-order variables are

$$\left.\begin{aligned} \mathscr{C}_1 &= \frac{-ik_z v_0}{(k^2+1)(1-\phi_0)} e^{i(k\cdot x-\omega t)}, \quad \psi_1^s = \frac{-\phi_0^2}{\xi}\frac{ik_x}{k^4} e^{i(k\cdot x-\omega t)}, \\ \mathscr{U}_1^s &= \frac{\phi_0 ik_z v_0}{k^2(k^2+1)(1-\phi_0)} e^{i(k\cdot x-\omega t)}. \end{aligned}\right\} \quad (39)$$

Figure 3(*b*) shows the perturbed melt velocity at the crest of a plane wave. The melt velocity superficially resembles the group velocity (figure 2) as the deflection of melt from the vertical is also controlled almost entirely by the elliptic term. Figure 3(*a*) shows the components of v_1 at the crest of a plane wave for the wave vector $k = 2i + 2k$. The two largest components of the melt velocity are the flux due to gravity, which drives the waves vertically, and a resistive 'compaction flux' driven by pressure gradients induced by volume changes of the viscous matrix. The compaction flux is

$$-\nabla \mathscr{C}_1 = \frac{-v_0 k_z}{(k^2+1)(1-\phi_0)}[k_x i + k_z k] e^{i(k\cdot x-\omega t)} \quad (40)$$

and is always normal to the wave front. The sum of the buoyancy flux and the deflecting compaction flux results in a net flow at an angle to both the vertical and the wave vector. Again, the compaction flux only becomes significant when the melt flux varies over the compaction length.

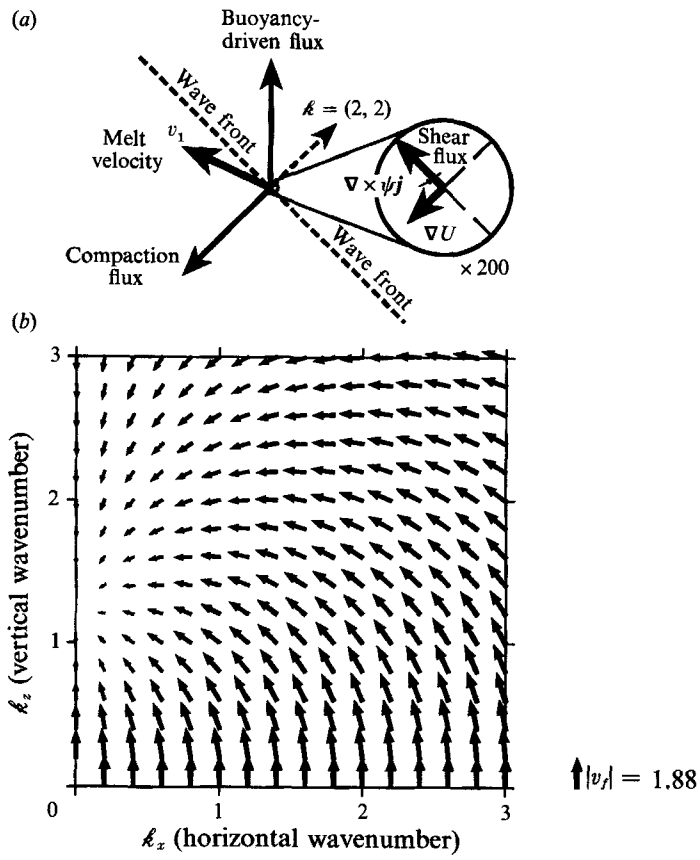

FIGURE 3. Perturbed melt (and matrix) velocity at the crest of the plane wave as given by (38). (*a*) Melt velocity vector for a plane wave with wave vector $k = 2i + 2k$ and $\phi_0 = 3\%$ showing components of the melt flux due to shear pressure gradients, compaction gradients, gravity and matrix velocity. The melt velocity vector, v_1, is primarily the sum of the vertical buoyancy-driven flux and the compaction flux and is at an angle to both the wave vector and the vertical. For this wave vector, the component of flow driven by pressure gradients produced by matrix shear is negligible. (*b*) Melt velocity vectors plotted against wavenumber ($\phi_0 = 3\%$). For $k_x k_z \neq 0$ this velocity includes a horizontal component. This deflection of the melt flux is almost entirely due to pressure gradients induced by volume changes of the viscous matrix.

Buoyancy and compaction pressure gradients dominate the melt flow at wavenumbers $k \gtrsim 1$. However, advection by the matrix flow and pressure gradients due to matrix shear also contribute to the melt velocity. The magnitude of these terms is readily estimated using (38) and (39) and is useful for determining under what circumstances these processes become significant. Rotational matrix flow driven by horizontal porosity gradients, $\nabla \times \psi_1^s j$, becomes important for $k_x \neq 0$ and wavenumbers comparable to the characteristic porosity ϕ_0. For melt extraction from the mantle, characteristic porosities may only be of the order of a few percent; therefore, rotational matrix convection will be sensitive to the longest-wavelength porosity variations. The previous section, however, suggests that porosity waves are sensitive to the shortest-wavelength porosity variations. This large difference in lengthscales may allow the two types of behaviour to be decoupled to a first approximation (see §4.3). In particular, the additional pressure gradient due to this incompressible flow (second term on the right-hand side of (38)) has a magnitude on

the order of ϕ_0 for all wave vectors. Thus shear pressure gradients induced by convection are probably small, as has been suggested by Ribe & Smooke (1987) and Scott (1988). When matrix deformation is driven by boundary conditions, however, these pressure gradients can be significant (figure 1; Spiegelman & McKenzie 1987). Finally, the compressible perturbation to the matrix velocity field, $\nabla \mathscr{U}_1^s$, never exceeds $\sim \phi_0 v_0$ for all wave vectors and is probably negligible for small mean porosities.

This linearized problem demonstrates several important features of the governing equations. It shows that compressible flow is described by a dispersive wave equation for porosity in which porosity waves can travel faster than the melt in the pores. These waves exist because the fluid flux is an increasing function of porosity and the matrix is deformable. The waves propagate because regions of excess flux can 'push' their way through the matrix. Viscous resistance of the matrix to volume changes, however, causes porosity waves to disperse and produces the additional pressure gradients required to deflect melt around obstacles in the melt flux. Part 2 will show that the effect of the elliptic compaction rate term is analogous for the full nonlinear equations. However, in the full equations it causes initial conditions to disperse into nonlinear solitary waves. Before we consider the importance of this term in the full equations however, it is useful to note what happens if this term is neglected in the nonlinear equations.

4.3. *Nonlinear equations: the zero-compaction-length approximation*

This section presents two approximations that reduce the governing equations to a single nonlinear wave equation for porosity that can be solved using the method of characteristics. These approximate equations are useful for illustrating some of the gross time-dependent behaviour of the nonlinear equations for compressible flow.

The first approximation decouples the equations governing volume changes of the matrix from those governing porosity-driven convection. Equations (18)–(21) contain a single small parameter, the characteristic porosity ϕ_0. If we neglect terms of order ϕ_0, the governing equations become

$$\partial\phi/\partial t + V_0 \cdot \nabla = \mathscr{C} + \Gamma, \tag{41}$$

$$-\nabla \cdot k_\phi \nabla \mathscr{C} + \mathscr{C} = \nabla \cdot k_\phi [\xi' \nabla^2 V_0 - \boldsymbol{k}] + (\Delta\rho/\rho_f)\Gamma, \tag{42}$$

$$\nabla^4 \psi^s = 0, \tag{43}$$

where $V_0 = \nabla \times \psi^s \boldsymbol{j}$. Thus, in the limit of small porosity, changes in porosity have negligible effect on the large-scale matrix shear. The matrix is incompressible to zeroth order and shear is driven by boundary conditions or additional sources of vorticity. Other authors have also used this 'small-porosity approximation' and have shown that the effects of the ϕ_0 terms are small for many problems (Barcilon & Richter 1986; Scott 1988). The effects of including terms of order ϕ_0 are discussed in more detail in Part 2.

Given V_0 and Γ, the equations governing compressible two-phase flow reduce to two coupled equations for porosity and compaction rate. If we now neglect *a priori* the elliptic term in (42), these equations can be combined to form a single nonlinear wave equation for porosity:

$$\phi_t + \boldsymbol{v}_\phi \cdot \nabla\phi = (\rho_s/\rho_f)\Gamma, \tag{44}$$

where

$$\boldsymbol{v}_\phi = V_0 + \frac{\partial k_\phi}{\partial \phi}[-\xi' \nabla^2 V_0 + \boldsymbol{k}]; \tag{45}$$

$\boldsymbol{v}_\phi$ is the phase velocity at which porosity, rather than melt, is transported. Comparison to the melt velocity shows that except for the case where $\partial k_\phi/\partial\phi = k_\phi/\phi$, the melt and porosity do not travel together. For a simple power-law relationship between permeability and porosity, $k_\phi = \phi^n$, the melt and porosity velocities are the same only if $n = 1$.

Letting $\phi(\boldsymbol{x}, t) = \phi(\boldsymbol{x}(\tau), t(\tau))$, equation (44) can be written as a coupled system of first-order ODEs:

$$\dot{\phi} = (\rho_s/\rho_f)\Gamma, \tag{46}$$

$$\dot{t} = 1, \tag{47}$$

$$\dot{\boldsymbol{x}} = \boldsymbol{v}_\phi, \tag{48}$$

where $\dot{\phi} = \mathrm{d}\phi/\mathrm{d}\tau$. If $\boldsymbol{V}_0(\boldsymbol{x}, t)$ and $\Gamma(\boldsymbol{x}, t)$ are known, (46)–(48) can be solved immediately, although for general $\boldsymbol{V}_0$ and Γ solutions must be obtained numerically.

The physical interpretation of this approximation is straightforward. By neglecting any resistance of the matrix to changing volume, we are effectively assuming that the compaction length δ is identically zero. This can be seen by rescaling the equations by a finite lengthscale d and letting $\delta \to 0$. The net result is to remove the only lengthscale in the problem. Therefore any initial condition for porosity simply evolves along a unique path in space and time independently of the porosity on neighbouring characteristics. Given a matrix flow field and a melting rate field, the evolution of any initial porosity distribution is completely determined.

The utility of this approximation is that it allows rapid solution of time-dependent nonlinear problems with arbitrary initial conditions. This method also accommodates multi-dimensions, melting and matrix deformation with equal ease, and is useful for demonstrating much of the basic behaviour of flow in deformable porous media. This approximation, of course, only remains accurate for problems where the viscous resistance term remains negligible. For many initial conditions, the following sections will demonstrate that this approximation leads to the development of porosity shock waves. In the vicinity of a shock wave, viscous resistance to volume changes cannot be negligible and the approximation breaks down. Nevertheless, while this approximation is not uniformally valid, it does provide a quick method for quantifying if, where, and when viscous resistance to volume changes becomes important. The following sections will briefly identify the conditions for shocks to form in a variety of geometries.

4.4. *Porosity shock waves: one and two dimensions, no melting*

The existence of porosity shock waves is most easily demonstrated from the one-dimensional equations without melting. Under these conditions, (44) with $k_\phi = \phi^n$ becomes

$$\phi_t + v_\phi \phi_z = 0, \tag{49}$$

where

$$v_\phi = W_0 + n\phi^{n-1}$$

and $W_0 = \text{const.}$ ($\phi_0 \ll 1$). Equation (49) has the general solution $\phi = \phi(z - v_\phi t)$ (e.g. Dodd *et al.* 1982). Because v_ϕ is an increasing function of ϕ, for $n > 1$, porosity shocks will form (in an infinite medium) from any initial condition where the porosity decreases in the direction of flow. This result has been pointed out for a similar set of equations by Toramaru (1988) and is typical of nonlinear wave equations (e.g. Dodd *et al.* 1982; Drazin & Johnson 1989). Figure 4 shows porosity profiles and

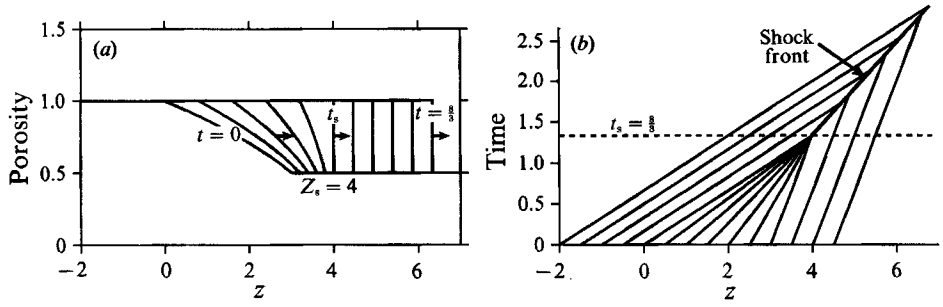

FIGURE 4. (*a*) Porosity profiles and (*b*) characteristics to illustrate the development of shocks in one dimension without melting. This initial condition ($t = 0$) was chosen to produce a perfect step ($\phi_{\max} = 1$, $\phi_1 = 0.5$) at $t = \frac{4}{3}$, $z = 4$ (see (1), Part 2). Without viscous resistance to compaction, this step function travels with permanent form at a phase velocity of $c_s = 1.75$. Note $c_s > 1$ is greater than the fastest melt velocity.

characteristics for an initial condition chosen to form a simple step-function shock (see (1) in Part 2).

This example and (44) and (46) assume that the permeability is a function only of porosity. More generally, the permeability can depend on additional properties of the matrix such as a spatially varying grain size. Inclusion of these additional parameters adds new source terms to the right-hand sides of (44) and (46). Therefore, even without melting, porosity need not be constant on characteristics. Nevertheless, these more general equations can still be solved using characteristics to show that, without melting, it is the melt flux (rather than porosity) that is conserved on the characteristics. Thus the more general criteria for shocks to form in one dimension without melting are that the partial derivative of the melt flux with respect to porosity, $\partial q/\partial\phi$, be an increasing function of porosity and that the melt flux decrease in the direction of flow. Inspection of (1) shows that constant-melt flux solutions are also the only steady-state solutions if there is no melting. This result implies that any perturbation to steady state will propagate as porosity waves. These results can be developed rigorously using characteristics (Spiegelman 1989).

In two and three dimensions, the shock condition is less easy to generalize as the 'direction of flow' is not well defined. Inspection of (45) shows that both the speed and direction of porosity transport depends on ϕ if there is incompressible matrix shear. Nevertheless, in two dimensions, (45) can be solved by inspection if melting is neglected. For $\Gamma = 0$ (and the condition that the permeability is solely a function of ϕ), (46) requires that porosity remains constant on a characteristic. Moreover, in two dimensions the small-ϕ_0 approximation implies that $\boldsymbol{V}_0 = \nabla \times \psi_0^s \boldsymbol{j}$. Substituting into (45) and integrating shows that porosity propagates along contours of the function

$$\psi_\phi(x,z) = \psi_0^s + (\partial k_\phi/\partial\phi)\,(\xi'\nabla^2\psi_0^s + x). \tag{50}$$

This solution can also be derived using characteristics. If ψ_0^s is steady in time, then contours of ψ_ϕ form the projection of the characteristics in the (x,z)-plane. If ψ_0^s is time dependent, then streamlines of ψ_ϕ show only the instantaneous direction of porosity transport. Comparison to the melt stream function for incompressible two-phase flow (§4.1)

$$\psi^f(x,z) = \psi_0^s + (k_\phi/\phi)\,(\xi'\nabla^2\psi^s + x), \tag{51}$$

shows that porosity behaves in a similar manner to the melt but does not travel with the melt if the permeability is not linearly proportional to porosity. Figure 5(*a*)

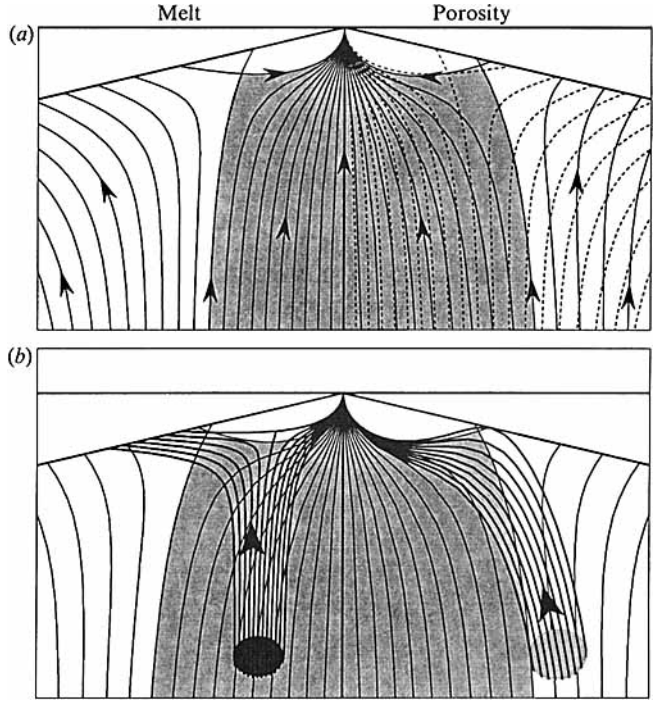

FIGURE 5. Initial conditions and porosity trajectories for the simple corner flow solution. (*a*) Melt and porosity trajectories for the constant-porosity initial condition shown in figure 1. The left-half shows the trajectories that a tracer travelling in the melt would follow. The right-half shows porosity trajectories (melt trajectories are dashed). These are the paths that an infinitesimal perturbation to constant porosity would travel on in the absence of viscous resistance to volume changes. Note that porosity trajectories resemble melt streamlines but in general behave as if the permeability were higher. When the initial condition is constant porosity, the trajectories meet only at the singularity and this initial condition is stable. (*b*) The left-half shows porosity trajectories for an initial porosity minimum that is $\frac{1}{3}$ of the constant background porosity ϕ_0. The right-half shows trajectories for an initial porosity maximum that is $3\phi_0$. The excess porosity travels towards the corner creating shocks where the higher porosity would coincide with the background porosity. For the negative perturbations, shocks would form further off axis as the initial obstruction is transported primarily by the matrix.

shows the trajectories of both melt and porosity for the two-phase corner flow solution from figure 1. The Appendix presents an analysis for the equilibrium transport of chemical trace elements and shows that chemical signals propagate along similar types of trajectories; however, even the most incompatible trace element can only travel as fast as the melt and therefore, in two (and three) dimensions, volume and chemistry do not travel together.

The potential for an arbitrary two-dimensional initial condition to form shocks is readily assessed given the porosity trajectories in the (x, z)-plane. As these flow lines are the projection of characteristics, a necessary (but not sufficient) condition for shocks to form is that the flow lines intersect one or more times for a given initial condition. If the trajectories coincide for different porosities, the problem reduces to the one-dimensional, no-melting problem and shocks develop from any region where the melt flux decreases in the direction of flow. Figure 5(*b*) illustrates these points using the corner flow solution and shows porosity trajectories for a finite-amplitude excess in porosity and for a local porosity minimum. In both cases, this figure suggests that any local perturbations to a steady-state flux will develop shocks. For

simplicity, this figure only shows the superposition of trajectories for the perturbations and the background flux, rather than the position of the actual shock front with time. In principle, the shock position can be calculated by conservation of mass. However, once shocks form, viscous effects become significant and unless the shock front is easy (or necessary) to calculate, it is more useful to solve the full equations. In Part 2, the behaviour of the full equations will be compared to that of the zero-compaction-length approximation for some initial conditions that produce simple shocks.

4.5. *Consequences of melting: zero-δ approximation*

Without melting, the rough rule is that shocks will form from any obstruction in the melt flux. This section shows that shock solutions also exist in the zero-compaction-length approximation when melting is included; however, the criterion for shocks to form changes. Adding the effects of mass transfer between solid and liquid is straightforward in the zero-compaction-length approximation. To produce analytic solutions, however, here we consider only one-dimensional problems where the melting rate field is assumed known and steady state ($\Gamma = \Gamma(z)$). Under these conditions, (46) and (48) form an autonomous system in ϕ and z and can be combined to remove τ such that

$$\mathrm{d}\phi/\mathrm{d}z = (\rho_\mathrm{s}/\rho_\mathrm{f})\,\Gamma/v_\phi.$$

Integrating once yields a relationship for the 'differential melt flux'

$$q_\mathrm{m}(\phi, z) = \phi W_0 + k_\phi - \frac{\rho_\mathrm{s}}{\rho_\mathrm{f}} \int \Gamma \,\mathrm{d}z. \tag{52}$$

This flux is simply the difference between the local melt flux, $q = \phi W_0 + k_\phi$ and the total amount of melt produced up to the height z. In one dimension without melting, the melt flux is conserved along characteristics. More generally, it is the differential flux. Thus, given any initial porosity ϕ_i at position z_i, it simply propagates along the contour $q_{\mathrm{m,i}} = q_\mathrm{m}(\phi_\mathrm{i}, z_\mathrm{i})$, i.e. contours of the function q_m are projections of the characteristic curves in the (ϕ, z)-plane. Comparison to (44) in one dimension shows that contours of q_m are just the set of all one-dimensional steady-state solutions with boundary condition $\phi(z_\mathrm{i}) = \phi_\mathrm{i}$. More physically, melt extraction balances production everywhere in steady state. Any initial condition for which q_m is not constant must evolve in time. The time spent on a contour to travel from initial position z_i to z is calculated from (47) and (48):

$$t(z, z_\mathrm{i}) = \int_{z_\mathrm{i}}^{z} \frac{\mathrm{d}z'}{v_\phi(\phi(z', q_{\mathrm{m,i}}))}, \tag{53}$$

where $\phi(z, q_{\mathrm{m,i}})$ is calculated from the inverse of (52) given $k_\phi(\phi)$ and Γ. $t(z, z_0)$ are the characteristic curves. The following sections present a few specific examples to demonstrate how mass transfer modifies the behaviour of shocks in the zero-compaction-length approximation.

4.6. *Examples: melting and shocks*

The simplest geometry in one dimension with a fixed amount of total melting is a single region of length d with a constant melting rate

$$\Gamma = \begin{cases} 0, & z < 0 \\ \Gamma_0, & 0 < z < d \\ 0, & z < d. \end{cases} \tag{54}$$

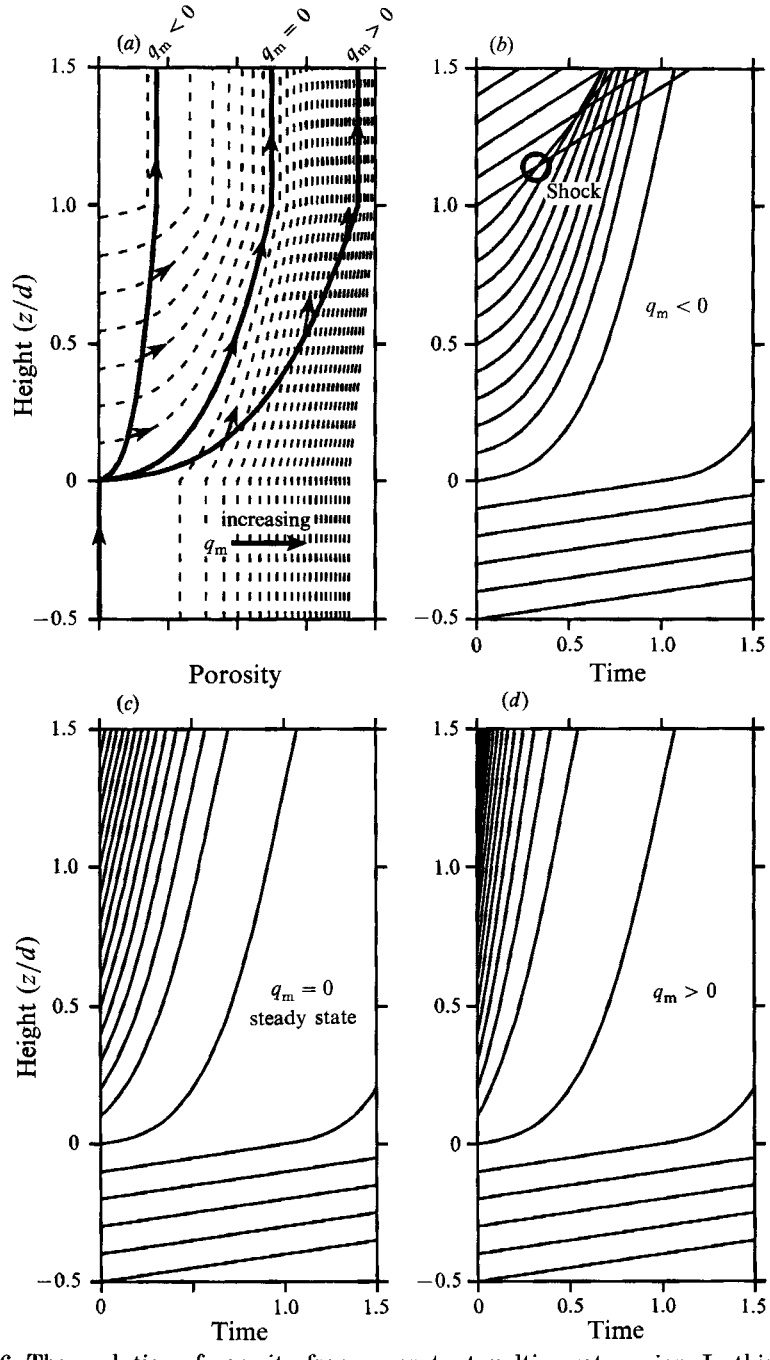

FIGURE 6. The evolution of porosity from a constant-melting-rate region. In this figure, melting occurs at a constant rate between $z/d = 0$ and 1. $\Gamma = 0$ outside of this region. (*a*) The initial porosity profiles (solid curves) for $q_m \leqslant 0$, $q_m = 0$ and $q_m \geqslant 0$, superposed on contours of $q_m(\phi, z)$ (dashed curves). The arrows indicate the direction of evolution. (*b*) Characteristic curves for the initial condition in (*a*) with $q_m \leqslant 0$. This initial condition grows to steady state but develops shocks immediately above the melting zone. (*c*) $q_m = 0$ is the steady-state solution. (*d*) $q_m \geqslant 0$, characteristics diverge with time resulting in smooth evolution to steady state. Inspection of (*a*) shows that all local perturbations about steady state propagate as nonlinear waves and produce shocks.

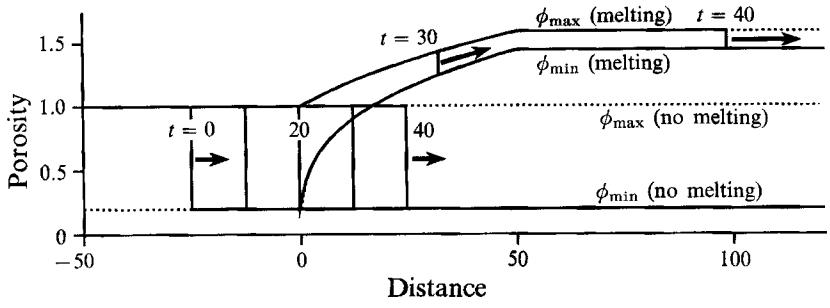

FIGURE 7. The effect of melting (and freezing) on shocks. The dotted curves show porosity trajectories (ϕ_{min} and ϕ_{max}) with and without melting included. The solid curves show the position of the porosity shock at times $t = 0$–40. In the constant-melting-rate field ($\Gamma = \Gamma_0$ for $0 < z < 50$), porosity increases on both trajectories and the spacing between trajectories decreases. Thus melting causes shocks to speed up but decrease in amplitude. Nevertheless because the transport velocity is always greater for larger values of q_m, once a shock forms, it always remains a shock. For $z > 50$ ($\Gamma = 0$) trajectories are again parallel but at a higher porosity with a smaller jump in porosity. Note if the arrows are reversed ($z \to -z$, $\Gamma \to -\Gamma$) this figure shows the effect of freezing on a small-amplitude shock.

Figure 6(*a*) shows the contours of $q_m(\phi, z)$ for this geometry and shows three initial conditions for porosity superposed on these contours. To evaluate the evolution of any given initial condition, just follow the porosity trajectories along which it propagates. For the curve marked $q_m < 0$, porosity will increase rapidly in the melting zone, but not above, producing a shock in the region immediately above the melting zone (figure 6*b* shows the characteristics for this initial condition). The initial condition with $q_m = 0$ is in steady state and no shocks form, although any local perturbation to this steady state, will generate at least transient shocks in the zero-δ approximation. Finally, the curve marked $q_m > 0$ has the differential flux everywhere increasing in the direction of flow, which simply relaxes to steady state without producing shocks.

These results imply that the inclusion of mass transfer changes the criteria for shocks to form but does not rule out the existence of shocks. Figure 6 shows that melting can actually enhance the development of shocks. For the initial condition where $q_m < 0$, shocks form from an initial condition where the flux q always increases in the direction of flow. In the absence of melting, no shocks would develop from this profile. For this particular initial condition and melting-rate function, the shock forms in the region where $\Gamma = 0$; however, it is straightforward to choose simple melting functions where locally the melt production exceeds extraction and shocks form even in the presence of melting. Spiegelman (1989) presents several examples.

For a shock in a melting region, the effects of mass transfer on the behaviour of the shock is evident from the porosity trajectories. Figure 7 shows the evolution of a step-function shock as it passes through a constant-melting-rate zone. As the transport velocity is always greater for larger values of q_m, once a shock forms, it must remain a shock. The principal consequences of melting are to increase the minimum porosity (and therefore the shock speed), while decreasing the difference between the maximum and minimum porosity. Thus shocks will tend to form more rapidly in melting regions, but be of smaller amplitude. Freezing will have precisely the opposite effect and cause small-amplitude shocks to slow down while growing in amplitude. This geometry is used in detail in Part 2 and is useful when we consider the effect of melting and freezing on the behaviour of solitary waves.

5. Discussion

The purpose of the simple analysis presented here is to demonstrate some of the basic physics of the equations governing flow in deformable permeable media. Rewriting the equations in potential form makes the structure of these equations clearer by distinguishing between compressible and incompressible matrix deformation. It should be stressed that both the solid and liquid phases are each individually incompressible to a first approximation; however, the volume fraction of solid and liquid can change. Incompressible matrix flow is governed by Stokes equations for porosity-driven convection while compressible matrix deformation is governed by a nonlinear wave equation for the evolution of porosity. As suggested by the linear analysis, these two modes of deformation act on very different lengthscales. Porosity-driven convection is sensitive to long-wavelength porosity variations and boundary conditions, whereas the porosity waves are sensitive to the compaction length.

Porosity waves are a fundamental feature of these equations. These waves propagate because variations in the melt flux force the matrix to change volume. As long as the flux is an increasing function of porosity and the matrix is deformable, then porosity waves will exist. The actual speed and behaviour of the porosity waves depends on the relationship between permeability and porosity. In the absence of any viscous resistance of the matrix to compaction, porosity waveforms are transported by the effective phase velocity, $v_\phi \propto \partial k_\phi/\partial\phi$ which arises from the matrix velocity and the divergence of the forced flux. If $\partial k_\phi/\partial\phi$ is also an increasing function of porosity, variations in melt flux will propagate as nonlinear waves and can steepen into shocks. For most commonly used permeability–porosity relationships, nonlinear waves are expected. In this case porosity variations do not travel with or transport melt, and generally travel faster and in different directions than any geochemical signal. For the full equations, several authors (Scott & Stevenson 1986; Scott 1988; Richter & Daly 1989) have shown that the solitary waves also travel faster than the melt in the pores (see also Part 2, Appendix B).

Without any resistive term in the equations, the nonlinearity of the melt flux with porosity can cause even smooth initial conditions to develop travelling discontinuities in flux. The zero-compaction-length approximation shows that porosity shocks will form from any local obstruction in the flux or from regions where melt is produced faster than it can be extracted. As these conditions are readily achieved for many geophysical problems, at least transient shocks are expected during melt extraction or in other deformable two-phase systems. For any given geometry and initial condition, the location, timing and amplitude of shocks can be calculated using characteristics and this analysis is readily extended to time-dependent problems, three-dimensions, and more complex melting/deforming systems.

It should be stressed that true 'shocks', actual discontinuities in porosity, would form only if the compaction length were identically zero (i.e. the matrix had no strength at all). For a small, but non-zero, compaction length, viscous resistance to volume changes cannot be negligible in a region of rapidly changing flux. If viscous resistance only modified the porosity structure near the shock (much like thermal diffusion modifies shocks in gas dynamics), then the zero-compaction-length approximation would be valid except within a few compaction lengths of the shock. However, linear analysis has already shown that viscous resistance causes plane waves to disperse. Using numerical techniques, Part 2 shows that the elliptic term causes dispersion into solitary waves in the full nonlinear equations. Because of this

dispersion, solutions to the full equations can differ significantly from the simple shock solutions. Thus the elliptic compaction term must be maintained to accurately describe the evolution of porosity. While the zero-compaction-length approximation is not uniformally accurate, it does rapidly quantify where viscous effects become important. By comparing the behaviour of the approximate and full equations for identical initial conditions, Part 2 will illustrate clearly how viscous effects modify the prediction of shocks.

Appendix. Behaviour of chemical tracers in viscous two-phase flows

Section 4.3 showed that the porosity and the melt do not travel together if the permeability is a nonlinear function of porosity. If $\partial k_\phi/\partial\phi$ is also an increasing function of porosity then porosity waves travel faster than the melt. This appendix shows that chemical tracers travel at most as fast as the melt and, therefore, signals in volume and chemical concentration do not travel together.

Neglecting chemical diffusion, the conservation of mass for an inert trace element that maintains chemical equilibrium between the solid and liquid phase is governed by

$$(\partial/\partial t)\,[\rho_{\rm f}\,\phi+\rho_{\rm s}(1-\phi)D]\,c^{\rm f}+\nabla\cdot[\rho_{\rm f}\,\phi\boldsymbol{v}+\rho_{\rm s}(1-\phi)\,D\boldsymbol{V}]\,c^{\rm f}=0, \tag{A 1}$$

where D is the partition coefficient that relates the concentration in the solid $c^{\rm s}$ to the concentration in the fluid $c^{\rm f}$. For trace elements we assume $c^{\rm s}=Dc^{\rm f}$. Setting D to be constant and using (1)–(3), (A 1) can be rewritten as

$$\frac{\partial c^{\rm f}}{\partial t}+\boldsymbol{v}_{\rm eff}\cdot\nabla c^{\rm f}=\frac{c^{\rm f}(D-1)\,\Gamma}{\rho_{\rm f}\,\phi+\rho_{\rm s}(1-\phi)}, \tag{A 2}$$

where

$$\boldsymbol{v}_{\rm eff}=\boldsymbol{V}-\left(\frac{1}{1+D'}\right)\frac{k_\phi}{\phi\mu}\nabla\mathscr{P},$$

and $D'=\rho_{\rm s}(1-\phi)D/(\rho_{\rm f}\,\phi)$ is the effective partition coefficient which is principally the ratio of D to the porosity. Equation (A 2) is a linear transport equation that can be solved using characteristics to show that any particle of tracer is simply transported by the effective velocity, $\boldsymbol{v}_{\rm eff}$. If $D'=0$ then $\boldsymbol{v}_{\rm eff}=\boldsymbol{v}$ and the tracer travels with the melt. As $D'\to\infty$, $\boldsymbol{v}_{\rm eff}\to\boldsymbol{V}$ and all of the tracer travels with the solid. In general, tracers with different partition coefficients travel along different characteristics; however, no tracer can travel faster than the melt. As shown earlier, for most reasonable forms of the permeability, porosity always travels faster and in different directions than the melt.

REFERENCES

Barcilon, V. & Lovera, O. 1989 Solitary waves in magma dynamics. *J. Fluid. Mech.* **204**, 121–133.

Barcilon, V. & Richter, F. M. 1986 Nonlinear waves in compacting media. *J. Fluid. Mech.* **164**, 429–448.

Batchelor, G. 1967 *An Introduction to Fluid Dynamics*. Cambridge University Press.

Bear, J. 1988 *Dynamics of Fluids in Porous Media*. Dover.

Brown, I. 1988 The compositional consequences of two phase flow. Ph.D. thesis, University of Cambridge.

Buck, W. R. & Su, W. 1989 Focused mantle upwelling below mid-ocean ridges due to feedback between viscosity and melting. *Geophys. Res. Lett.* **16**, 641–644.

CHEADLE, M. 1989 Properties of texturally equilibrated two-phase aggregates. Ph.D. thesis, University of Cambridge.

DALY, S. F. & RICHTER, F. M. 1989 Dynamical instabilities of partially molten zones: Solitary waves vs. Rayleigh Taylor plumes. *EOS Trans. Am. Geophys. Union* **70**, 499.

DIDWANIA, A. K. & HOMSY, G. M. 1981 Flow regimes and flow transitions in liquid fluidized beds, *Intl J. Multiphase Flow* **7**, 563–580.

DIDWANIA, A. K. & HOMSY, G. M. 1982 Resonant sideband instabilities in wave propagation in fluidized beds. *J. Fluid. Mech.* **122**, 433–438.

DODD, R., EILBECK, J., GIBBON, J. & MORRIS, H. 1983 *Solitons and Non-linear Wave Equations.* Academic.

DRAZIN, P. & JOHNSON, R. 1989 *Solitons: an Introduction.* Cambridge University Press.

DREW, D. 1971 Average field equations for two-phase media. *Stud. Appl. Maths* **50**, 133–166.

DREW, D. 1983 Mathematical modeling of two-phase flow. *Ann. Rev. Fluid Mech.* **15**, 261–291.

DULLIEN, F. 1979 *Porous Media Fluid Transport and Pore Structure.* Academic.

FOWLER, A. 1985 A mathematical model of magma transport in the asthenosphere. *Geophys. Astrophys. Fluid Dyn.* **33**, 63–96.

MCKENZIE, D. 1984 The generation and compaction of partially molten rock. *J. Petrol* **25**, 713–765.

PHIPPS MORGAN J. 1987 Melt migration beneath mid-ocean spreading centers. *Geophys. Res. Lett.* **14**, 1238–1241.

RABINOWICZ, M., NICOLA, A. & VIGNERESSE, J. 1984 A rolling mill effect in the asthenosphere beneath oceanic spreading centers. *Earth Planet. Sci. Lett.* **67**, 97–108.

RIBE, N. 1985 The deformation and compaction of partially molten zones. *Geophys. J. R. Astron. Soc.* **83**, 137–152.

RIBE, N. 1985*b* The generation and composition of partial melts in the earth's mantle. *Earth Planet. Sci. Lett.* **73**, 361–376.

RIBE, N. 1988*a* Dynamical geochemistry of the Hawaiian plume. *Earth Planet. Sci. Lett.* **88**, 37–46.

RIBE, N. 1988*b* On the dynamics of mid-ocean ridges. *J. Geophys. Res.* **93**, 429–436.

RIBE, N. & SMOOKE, M. 1987 A stagnation point flow model for melt extraction from a mantle plume. *J. Geophys. Res.* **92**, 6437–6443.

RICHTER, F. M. 1986 Simple models of trace element fractionation during melt segregation. *Earth Planet. Sci. Lett.* **77**, 333–344.

RICHTER, F. M. & DALY, S. F. 1989 Dynamical and chemical effects of melting a heterogeneous source. *J. Geophys. Res.* **94**, 12,499–12,510.

RICHTER, F. M. & MCKENZIE, D. 1984 Dynamical models for melt segregation from a deformable matrix. *J. Geol.* **92**, 729–740.

SAFFMAN, P. G. 1971 On the boundary condition at the surface of a porous medium. *Stud. Appl. Maths* **50**, 93–101.

SCHEIDEGGER, A. E. 1974 *The Physics of Flow Through Porous Media.* University of Toronto Press.

SCOTT, D. 1988 The competition between percolation and circulation in a deformable porous medium. *J. Geophys. Res.* **93**, 6451–6462.

SCOTT, D. & STEVENSON, D. 1984 Magma solitons. *Geophys. Res. Lett.* **11**, 1161–1164.

SCOTT, D. & STEVENSON, D. 1986 Magma ascent by porous flow. *J. Geophys. Res.* **91**, 9283–9296.

SCOTT, D. & STEVENSON, D. 1989 A self-consistent model of melting, magma migration, and buoyancy-driven circulation beneath mid-ocean ridges. *J. Geophys. Res.* **94**, 2973–2988.

SOTIN, C. & PARMENTIER, E. M. 1989 Dynamical consequences of compositional and thermal density stratification beneath spreading centers. *Geophys. Res. Lett.* **16**, 835–838.

SPARKS, D. W. & PARMENTIER, E. M. 1991 Melt extraction from the mantle beneath spreading centers. *Earth Planet. Sci. Lett.* **105**, 368–377.

SPIEGELMAN, M. 1989 Melting and melt migration: The physics of flow in deformable porous media. Ph.D. thesis, University of Cambridge.

SPIEGELMAN, M. 1990 Focusing on Freezing: A new mechanism for lateral melt migration at mid-ocean ridges. *EOS Trans. Am. Geophys. Union* **71**, 1829.

SPIEGELMAN, M. 1991 2-D or not 2-D: Understanding melt migration near a sloping, freezing boundary. *EOS Trans. Am. Geophys. Union* **72**, 265.

SPIEGELMAN, M. 1993 Flow in deformable porous media. Part 2. Numerical analysis – the relationship between shock waves and solitary waves. *J. Fluid. Mech.* **247**, 39–63.

SPIEGELMAN, N. & MCKENZIE, D. 1987 Simple 2-D models for melt extraction at mid-ocean ridges and island arcs. *Earth Planet. Sci. Lett.* **83**, 137–152.

TORAMARU, A. 1988 Formation of propagation pattern in two-phase flow system with application to volcanic eruption. *Geophys. J. R. Astra Soc.* **95**, 613–623.

VON BARGEN, N. & WAFF, H. S. 1986 Permeabilities, interfacial areas and curvatures of partially molten systems: Results of numerical computations of equilibrium microstructures. *J. Geophys. Res.* **91**, 9261–9276.